Nonlinear optical generation in a hydrogen discharge

D. W. Tokaryk,* G. Z. Zhang,† and B. P. Stoicheff
Department of Physics, University of Toronto and Photonics Research Ontario, Toronto, Ontario, Canada M5S 1A7
(Received 21 April 1998)

Sum-frequency generation with electromagnetically induced transparency (EIT) has been examined in a hydrogen discharge. EIT is demonstrated in the $3p$-$1s$ and $4p$-$1s$ transitions at 102.6 and 97.3 nm, respectively, with increased efficiency of generation arising from higher H-atom density, although competing effects due to the presence of H_2 distort the line shapes of these spectra. Only for shorter-wavelength transitions (such as $7p$-$1s$ and $8p$-$1s$) that show very large shifts and distortions is there a decrease in intensity in comparison with generated radiation from H atoms external to the discharge. [S1050-2947(99)01404-3]

PACS number(s): 42.65.Ky, 42.50.Hz, 42.50.Gy, 32.80.Fb

Over the last few years, experiments in this laboratory have shown that electromagnetically induced transparency (EIT) can be exploited to augment the production of vacuum-ultraviolet (VUV) and extreme-ultraviolet (XUV) radiation by four-wave frequency mixing in atomic hydrogen [1–6]. It has also been demonstrated that the intensity of generated radiation can be enhanced by increasing the value of the product NL, where N is the number density of atomic hydrogen, and L is the length of the atom-laser interaction path. In the earlier work, hydrogen atoms were produced in a discharge through molecular H_2 and drawn out of the discharge into the interaction region. In this paper we describe the results of frequency-mixing experiments conducted *within* the hydrogen discharge where the atom number density was found to be larger: the interaction length L was also increased, yielding much higher intensity of generated VUV and XUV radiation. The results within the plasma are compared with earlier work [4,6].

Most of the experimental details were similar to those presented in earlier work [6], except for the sample cell, which consisted of the central section of the Wood's discharge tube. This section of Pyrex tubing, 0.8 cm inner diameter and 10 cm length, was sealed with a quartz window at the laser input end, and drawn to a nozzle of 0.15 cm diameter at the output end. The nozzle was sealed to a copper flange attached to the vacuum chamber. Hydrogen gas, flowing through the Wood's tube was pumped through the nozzle and a hole (1 cm long and 0.2 cm diameter) bored through the flange. Copper was chosen for the flange since hydrogen atoms readily recombine on a copper surface [7] and could thus reduce the number density of hydrogen atoms in the beam path outside the discharge region. The discharge was run at a pressure of 0.7 Torr, with a voltage of ~2000 V and current of ~40 mA.

Two pulsed dye lasers were used, one for production of 243 nm radiation (multimode) to strike the $1s$-$2s$ two-photon resonance, and a single-mode laser to provide radiation for coupling of the $2s$ state to various np states. The 243-nm beam was produced by doubling 486 nm radiation in a β-barium borate crystal, giving pulsed radiation of 6 ns duration and a 0.20-cm^{-1} full width at half-maximum (FWHM)]. The coupling beam was amplified and collimated by passage through two Bethune-prism cells providing pulsed radiation of 9–16 ns duration (dependent on the dyes used for the selected Balmer wavelengths) with a linewidth of 0.02 cm^{-1} (FWHM). This radiation was admitted into the discharge tube without focussing: the beam diameter varied between 0.4 and 0.6 mm, for the different wavelengths. A lens of 36 cm focal length was used to focus the 243-nm beam in the center of the discharge tube where it produced an oval image with major and minor axes of ~0.32 and 0.25 mm, respectively. Further particulars regarding the laser systems are provided in Ref. [6].

By selecting the coupling-laser wavelength to coincide with Balmer transitions ($np \leftarrow 2s$), we have investigated nonlinear generation at the $3p$-$1s$, $4p$-$1s$, $7p$-$1s$, and $8p$-$1s$ transitions, also at high Rydberg transitions ($n \geqslant 24$), and in the region of the ionization continuum. In these experiments of frequency mixing within the plasma, we could not record photoion signals arising from multiphoton ionization of hydrogen atoms (as was done previously), so there was no longer a direct way to measure the linear susceptibility $\chi^{(1)}$ of the medium. However, we could observe optogalvanic signals from the discharge produced when the coupling laser was tuned to the np-$2s$ transitions, and these were useful for setting the coupling-laser frequency exactly on resonance.

In Fig. 1(a) is shown the $3p$-$1s$ spectrum generated near 102.6 nm, by scanning the two-photon laser frequency, with the coupling-laser frequency fixed to the $3p$-$2s$ resonance, and its energy at ~0.6 mJ per pulse. The most striking aspect of the spectrum is the sharpness of the central component with a width of ~0.3–0.4 cm^{-1} (FWHM), which is far narrower than the Doppler width of the $3p$-$1s$ transition (~1.5 cm^{-1}). Such spectral narrowing is characteristic of EIT-enhanced four-wave sum-mixing at high NL, as recently discussed by Hakuta and coworkers [8]. Our measured value for the breadth of the generated signal was limited by the width of the multimode envelope of the 243 nm laser radiation and is considered to be an upper limit.

The spectrum in Fig. 1(b) was taken under the same experimental conditions as that of Fig. 1(a), but with the coupling-laser frequency being scanned while the two-

*Present address: Dept. of Physics, Engineering and Geoscience, Mount Allison University, Sackville, NB, Canada E4L 1E6.
†Present address: New Focus Inc., Santa Clara, CA 95051-0905.

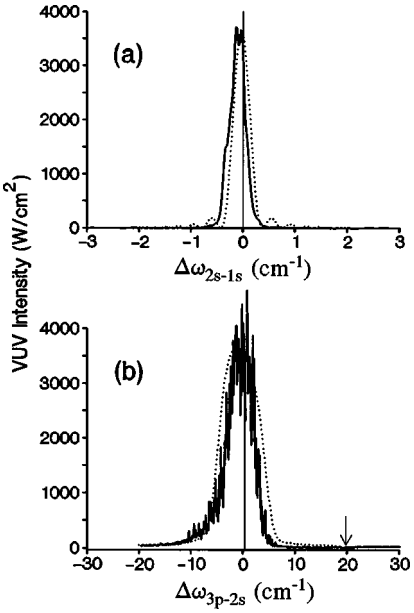

FIG. 1. Spectra of VUV radiation generated near the $3p$-$1s$ transition at 102.6 nm, obtained by scanning (a) the 243-nm laser and (b) the coupling-laser frequency. Calculated intensities are plotted vs frequency detunings, with observed and calculated spectra (dotted lines) normalized. The arrow indicates the position of the $P(1)$ line in the (6-0) band of the $B\,^1\Sigma_u^+ - X\,^1\Sigma_g^+$ transition in H_2.

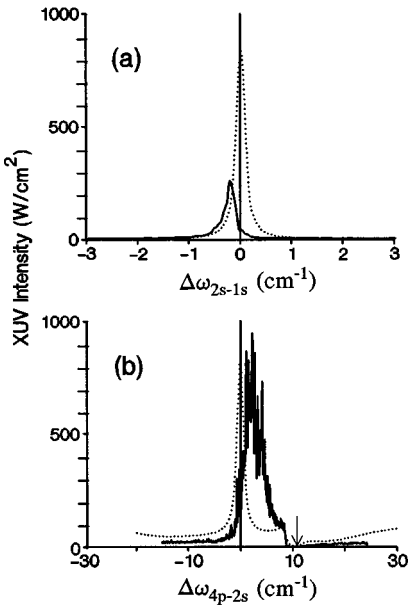

FIG. 2. Spectra of XUV radiation generated near the $4p$-$1s$ transition at 97.3 nm, obtained by scanning (a) the 243-nm laser and (b) the coupling-laser frequency. Calculated intensities are plotted vs frequency detunings, with observed and calculated spectra (dotted lines) normalized in (b) and the same scaling factor applied to the spectra in (a). The arrow indicates the position of the (11-0) band $R(1)$ line of the $B\,^1\Sigma_u^+ - X\,^1\Sigma_g^+$ transition in H_2.

photon frequency was fixed on resonance. The generated signal was much broader, with a noticeable drop to zero intensity when the coupling-laser frequency was approximately $+20$ cm^{-1} from the resonance. This drop in intensity is associated with the coexistence of molecular hydrogen [5,6] in the discharge. Here, the (6-0) band $P(1)$ line of the $B\,^1\Sigma_u^+ - X\,^1\Sigma_g^+$ transition in H_2 strongly reabsorbs the generated light resulting in a null in intensity, and the associated dispersion alters the phase-matching properties of the medium.

By comparing the observed with simulated spectra, we have tried to obtain estimates of four experimental parameters that could not be obtained by direct measurement, namely, the number densities of hydrogen atoms and of molecules (in the $v=0$, $J=1$ level of the ground state), the effective Doppler breadth, and the coupling Rabi frequency. Spectra were calculated using the procedures outlined in [3,5], based on the theory of Harris, Field, and Imamoglu [9]. Initial estimates of the Rabi frequency were obtained from measurements of the temporal and spatial characteristics of the coupling-laser beam. The Doppler width quoted above ($\sim$1.5 cm^{-1}) provided a starting point for estimation of the effective Doppler width, which in earlier work was found to vary with coupling laser intensity.

In the simulations, the observed width of the resonance in Fig. 1(a) was found to depend primarily on the coupling-laser Rabi frequency and the number-density of hydrogen atoms, but was significantly less sensitive to the other parameters. The simulated width approached the measured value for a density of $N\sim 2\times 10^{15}$ cm^{-3}, assuming a Rabi frequency of approximately 7–9 cm^{-1}. Estimates of the H_2 number density and Doppler broadening were obtained, and the value of the Rabi frequency was refined, by comparing simulations to the spectrum in Fig. 1(b), and to a spectrum scan (not shown) for which the coupling energy per pulse was much less, $\sim$0.2 mJ. Good agreement between the observed spectra of Figs. 1(a) and 1(b) and the simulations was obtained with atomic and molecular number densities of 2×10^{15} and 2×10^{14} cm^{-3}, respectively, with the Rabi frequency set to 8.0 cm^{-1}, and a Doppler width of 1.8 cm^{-1}, slightly larger than the initial estimate. Graphs of the calculated envelopes are shown for comparison with the observed spectra in Fig. 1, where calculated values of intensities are used on the ordinate axis. These results indicate that the atomic hydrogen number density within the discharge is an order of magnitude greater than the value estimated in earlier work for hydrogen density outside the discharge.

In Fig. 2 are shown XUV-generated $4p$-$1s$ spectra near 97.3 nm, one being a two-photon scan with the coupling-beam wavelength fixed to the $4p$-$2s$ resonance (486.1 nm), and the other a coupling-laser scan with the two-photon frequency fixed to the $1s$-$2s$ resonance. The experimental conditions were identical to those presented above, except that the coupling-laser energy per pulse was slightly higher at 0.7 mJ for both spectra. Once again, the two-photon scan revealed only a single sharp component, but with its peak intensity shifted $\sim$0.2 cm^{-1} from resonance. In the coupling-laser scan, the generated signal is much broader and asymmetric, and is also shifted from resonance (by $\sim$2 cm^{-1}). A strong absorption approximately -11 cm^{-1} from the $4p$-$1s$ resonance center is attributed to the (11-0) band $R(1)$ line of the $B\,^1\Sigma_u^+ - X\,^1\Sigma_g^+$ transition in H_2. This molecular transition affects the phase-matching properties of the medium, resulting in a slight asymmetry and frequency shift in the generated radiation (compare with Fig. 5 of [6]), but is not the main cause of the observed shift. Both spectra in Fig.

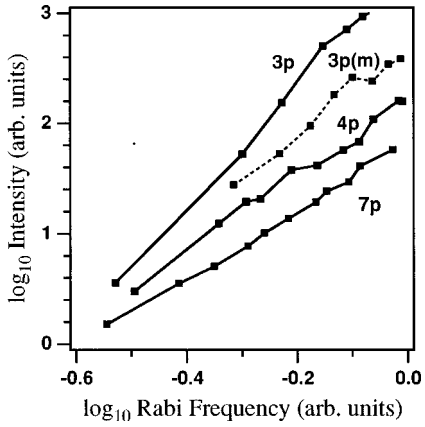

FIG. 3. A graph of the dependence of generated intensities on the Rabi frequencies of $3p$-$2s$, $4p$-$2s$, and $7p$-$2s$ coupling laser beams. In this log-log plot, the abscissa values are proportional to the Rabi frequencies. All data were obtained with the two-photon and coupling-laser frequencies on resonance, and the coupling laser operating in single mode, except for the data labeled $3p(m)$ for which the coupling laser was deliberately run in three longitudinal modes simultaneously.

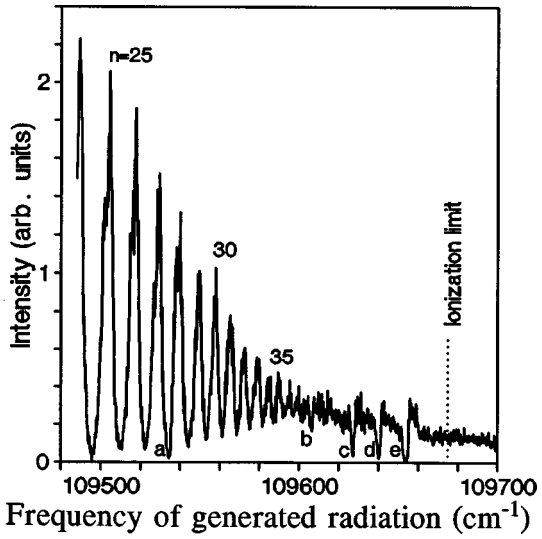

FIG. 4. Spectrum of generated XUV radiation near the ionization limit of atomic hydrogen. Absorption features attributed to molecular hydrogen include *a*, the Lyman band 19-0 $R(2)$ line; *b*, the Werner band 8-1 $Q(2)$ line; *c*, unknown; *d*, the Werner band 8-1 $Q(1)$ line; and *e*, the Lyman band 19-0 $P(1)$ line.

2 were simulated with the same atomic and molecular number densities given for the $3p$-$1s$ simulations, a larger Doppler width of 2.0 cm^{-1} (to account for the higher generated frequency), and an effective Rabi frequency of 4.2 cm^{-1}. In Fig. 2(b), the intensities were normalized, while in Fig. 2(a) the observed intensity appears to be only 25% of the simulated value, yet it is in agreement with the intensity on resonance in Fig. 2(b), namely, when $\Delta\omega_{4p\text{-}2s}=0$. It is noted that, in the scans of Fig. 2, the fixed frequencies were set on resonance within the plasma by making use of optogalvanic signals.

Four-wave sum-mixing experiments were also performed with the coupling laser frequency scanned through the $7p$ and $8p$ levels, and some enhancement due to EIT was observed. Again, in the spectra for two-photon scans, the generated signals consisted of single peaks of narrow width, shifted slightly off resonance. However, the spectra for coupling-laser scans were broad and distorted, with large shifts ($\sim$5 cm^{-1}) from resonance. Such effects could occur because of the presence of free electrons and the hydrogen species (H_2, H_3, and their ions) in the plasma. Their presence in sufficient quantities could affect the linear and nonlinear susceptibilities of the medium, and alter the phase matching and possibly cause absorption of the generated radiation. However, the density of free electrons required to produce a plasma frequency in the VUV region is estimated to be of the order of 10^8 times the H-atom density, which seems unlikely in the present discharge. Also, since the VUV and XUV spectra for all but H and H_2 are not known, their direct influence could not be calculated. The magnitude of competing effects may be more prominent in the weak $7p$ and $8p$ spectra, whereas in the much more intense $3p$ and $4p$ spectra the EIT generation process may be sufficiently strong to mask any perturbations due to the presence of other species in the plasma.

While we could not confirm directly that EIT played a role in enhancement of the generation process in the discharge, since probe radiation at 97.3 and 102.6 nm was not available, nor could ion measurements be carried out as in the earlier experiments, indirect evidence suggests that EIT was effective. First, the sub-Doppler widths observed when the two-photon laser frequency was scanned with the coupling-laser frequency fixed on resonance, were consistent with EIT effects [8]. Second, spectra for both the coupling and the two-photon laser-scans were well represented by simulations calculated using EIT formalism; and third, the intensities of the incident laser beams used in this experiment were comparable to those used in the earlier work, where the influence of EIT was conclusively demonstrated. Most convincing of all, however, was the dependence of the generated VUV/XUV intensity on the incident coupling-laser intensity, shown in Fig. 3. For these measurements, the frequencies of both lasers were fixed to their respective resonances.

The results are displayed on a $\log_{10}$-$\log_{10}$ plot for data involving the $3p$, $4p$, and $7p$ levels, with the square-root of the energy per pulse plotted as abscissa, in order to be proportional to the coupling Rabi frequency. When straight lines were fitted to the linear regions of these data, the slopes were $\sim$5.7, 3.3, and 2.9. In each case, the value is greater than 2.0, the slope expected for the output intensity being directly proportional to the intensity of the coupling-laser beam. This result implies that the strong coupling-field produces EIT and results in enhancement of the nonlinear process. In Fig. 3, comparison is also made of generated intensities involving the $3p$ level taken with the coupling-laser beam operating in single mode, with data for the laser deliberately misadjusted to run in three longitudinal modes having a separation of 0.15 cm^{-1}. The slope of the log-log plot is reduced from 5.7 to 4.0 indicating that enhancement due to EIT is reduced by mode beating in multimode operation.

The measured ratio for the $3p$-$1s$ and $4p$-$1s$ peak intensities generated in the discharge (Figs. 1 and 2) gave a value of $\sim$10:1, while calculations predicted a ratio of $\sim$5.6:1. It was also of interest to compare the peak intensities of the $4p$-$1s$ XUV spectra within the discharge (Fig. 2), with those

of the earlier measurements taken with a 5-cm length of hydrogen atoms outside the discharge. For comparable coupling-laser Rabi frequencies, the ratio of peak intensities was measured to be ~25:1 in favor of the discharge data, while the simulations predicted a value of ~16:1. These comparisons of measured intensities are approximations only, for a number of reasons: first, the bias voltage on the electron-multiplier tube used in the intensity measurements was very low to avoid saturation, and the tube sensitivity in this low-voltage regime had to be extrapolated from the manufacturer's specification sheet, and second, comparisons of data from the discharge with data from our previous work involved an estimate of geometric factors resulting from cell design and from different placement of the cells relative to the entrance slit of the spectrometer. Given these limitations, the comparisons of relative intensities are reasonably good.

Generated XUV light was observed from higher Rydberg levels, with $n=24$ up to 36, and in the continuum above the ionization limit (Fig. 4), but EIT was not a factor in this region. These spectra were simulated by calculating both $\chi^{(3)}$ and $\chi^{(1)}$ for atomic hydrogen [10], using the first 100 discrete levels and the continuum up to 10 times the ionization potential of hydrogen. The results are in good agreement with our observations (except for a range of ± 10 cm^{-1} near the ionization limit, where the effects of the truncated set of discrete levels were most noticeable). Several absorption lines were observed in the spectrum and have been assigned to transitions in H_2 involving the $v=0$ and $v=1$ levels of the $X\,^1\Sigma_g^+$ ground state. These absorptions were observed in the plasma, where various excitation mechanisms can populate higher levels of H_2, but were not detected in our previous experiments with hydrogen outside the discharge region.

We have demonstrated electromagnetically induced transparency in hydrogen atoms within a hydrogen plasma, resulting in a large increase in effiency of VUV and XUV generation due to four-wave sum mixing. While the observed spectra of the VUV and XUV radiation may be more difficult to describe due to the presence of H_2^+, H_3, and H_3^+, in the plasma, the increased hydrogen atom number density (and laser-atom interaction length) results in much more intense radiation than we have previously been able to achieve.

This research was supported by the Natural Sciences and Engineering Research Council of Canada, Technology Ontario, and the University of Toronto.

[1] K. Hakuta, L. Marmet, and B. P. Stoicheff, Phys. Rev. A **45**, 5152 (1992).
[2] G. Z. Zhang, K. Hakuta, and B. P. Stoicheff, Phys. Rev. Lett. **71**, 3099 (1993).
[3] R. I. Thompson, B. P. Stoicheff, G. Z. Zhang, and K. Hakuta, Appl. Phys. B: Lasers Opt. **60**, S129 (1995).
[4] G. Z. Zhang, M. Katsuragawa, K. Hakuta, R. I. Thompson, and B. P. Stoicheff, Phys. Rev. A **52**, 1584 (1995).
[5] M. Katsuragawa, G. Z. Zhang, and K. Hakuta, Opt. Commun. **129**, 212 (1996).
[6] G. Z. Zhang, D. W. Tokaryk, B. P. Stoicheff, and K. Hakuta, Phys. Rev. A **56**, 813 (1997).
[7] B. J. Wood and H. Wise, J. Chem. Phys. **29**, 1416 (1958).
[8] R. S. D. Sihombing, M. Katsuragawa, G. Z. Zhang, and K. Hakuta, Phys. Rev. A **54**, 1551 (1996).
[9] S. E. Harris, J. E. Field, and A. Imamoglu, Phys. Rev. Lett. **64**, 1107 (1990).
[10] D. C. Hanna, *Nonlinear Optics of Free Atoms and Molecules* (Springer-Verlag, Berlin, 1979).